様式 2-4-1

日米科学技術協力事業「脳研究」分野
グループ共同研究実施報告書　　〔研究分野：2〕

１．グループ共同研究代表者
所属機関・職名・氏名
自然科学研究機構　岡崎統合バイオサイエンスセンター神経分化研究部門　教授　岡村康司

２．研究課題名
電位依存性チャネルの機能修飾と集積機構

３．日本側グループ組織（代表者及び分担者の所属・職・氏名）
代表者：自然科学研究機構岡崎統合バイオサイエンスセンター・教授・岡村康司
分担者：山形大学医学部発達生体防御学講座小児医科学分野・教授・早坂清
分担者：自然科学研究機構生理学研究所・助手・岩崎広英
分担者：山形大学医学部発達生体防御学講座小児医科学分野・医局員・白幡恵美
分担者：自然科学研究機構生理学研究所・博士研究員・佐々木　真理
分担者：自然科学研究機構生理学研究所・教授・池中一裕
代表者：自然科学研究機構岡崎統合バイオサイエンスセンター・助教授・東島眞一
分担者：埼玉医科大学生理学教室・講師・中平健祐
分担者：日本学術振興会特別研究員・西野敦雄
分担者：日本学術振興会特別研究員・村田喜理

４．米国側グループ組織（代表者及び分担者の所属・職・氏名）
James S. Trimmer , Department of Pharmacology, University of California at Davis, Professor
Hiroaki Misonou, University of Maryland, Assistant Professor

５．研究期間　平成１６年４月１日～平成１８年３月３１日

６．研究の概要，成果及び意義（1000 字）
電位依存性チャネルの集積機構とその生理的意義に関する共同研究を行ってきた。とくに神経系に幅広く存在する電位依存性 Nav チャネルに焦点をあて、主に生化学的手法と電気生理学的手法を用いて発現制御機構の解析を行った。まず山形大学早坂教授らがクローニングしたヒト Nav1.6 チャネルの機能発現実験を可能とし、神経細胞軸索ランビエ絞輪や起始部での Nav チャネル分子の集積を再構成する系を確立することを目指した。この結果、裏打ち蛋白であるアンキリンGが Nav1.6 チャネル分子の集積を促進するだけでなく、Nav チャネルのゲーティングの性質をも制御する（不活性化の遅い成分を減少させる）という知見を得た。このことは、これまで考えられてきたようにアンキリンはイオンチャネルの集積により興奮性を制御するだけでなく、直接チャネルの分子特性を変化させることによっても制御しているという重要な可能性を示した、脱髄疾患などでの興奮性の異常のメカニズムを説明できる点で、意義が大きい。また、これらの分子制御機構を多種の動物間で比較することにより明らかにするため、①尾索動物のイオンチャネルゲノム情報を用いて運動機能におけるイオンチャネル発現プロファイルの解析および運動制御におけるイオンチャネル機能の解析、②トランスジェニックゼブラフィッシュを用いた神経回路機能とイオンチャネルに関する研究（Joe Fetcho ラボによる協力）も行った。

７．その他（実施上の問題点，特記事項等）
アンキリン G と Nav1.6 分子との相互作用は他のイオンチャネルの場合と同様弱く、生化学的に相互作用を検出することができていない。James Trimmer 側が提供した Nav1.6 に対する抗体により蛋白を検出することは可能であったが、今後 Trimmer

博士の研究室で新たなモノクローナル抗体を作成することになっており、生化学的なアンキリンGと Nav1.6 分子との相互作用の検出を目指す予定である。更に今回 Trimmer 博士との間で築かれた交流は、我々が最近同定したイオンチャネル関連蛋白である電位依存性ホスファターゼ (Murata et al, 2005) 及び電位依存性プロトンチャネル(Sasaki et al, 2006)の分子機能の解明においても共同研究のプラットフォームの構築に到る可能性が期待される。なお、本研究プロジェクト遂行にあたっては、Duke 大学の Vann Bennett 教授に多大なる協力を得た。また、ペンシルバニア大学の Edward Cooper 博士、コーネル大学の Joe Fetcho 博士、ワシントン大学の Jianmin Cui 博士との研究交流によっても行われた。

◎参考資料があれば，添付ください。
本研究プロジェクトと関連して発表された論文は以下のものである。

Ohtsuka Y, Okamura Y. Voltage-dependent calcium influx mediates maturation of myofibril arrangement in ascidian larval muscle. **Developmental Biology**, in press

Kimura Y, Okamura Y, Higashijima S. alx, a zebrafish homolog of Chx10, marks ipsilateral descending excitatory interneurons that participate in the regulation of spinal locomotor circuits. **J Neurosci** (2006)

Shirahata E, Iwasaki H, Takagi M ,Lin C, Bennett V, Okamura Y, Hayasaka K. Ankyrin-G regulates inactivation gating of the neuronal sodium channel, Nav1.6 **J Neurophysiol**(2006)

Sasaki M, Takagi M, Okamura Y .A voltage sensor-domain protein is a voltage-gated proton channel. **Science**(2006)

Murata Y, Iwasaki H, Sasaki M, Inaba K, Okamura Y. Phosphoinositide phosphatase activity coupled to an intrinsic voltage sensor. **Nature**(2005)

Okamura Y, Nishino A, Murata Y, Nakajo K, Iwasaki H, Ohtsuka Y, Tanaka-Kunishima, M, Takahashi N, Hara Y, Yoshida T, Nishida M, Okado H, Watari H, Meinertzhagen I.A, Satoh N, Takahashi K, Satou Y, Okada Y, Mori M. Comprehensive analysis of the ascidian genome reveals novel insights into the molecular evolution of ion channel genes.**Physiological Genomics**(2005)

Miyamoto T, Morita, K, Takemoto, D, Takeuchi, K, Kitano, Y, Miyakawa, T, Nakayama, K, Okamura, Y,Sasaki, H, Miyachi, Y, Furuse, M, Tsukita, S. Tight junctions in Schwann cells of peripheral myelinated axons: a lesson from claudin-19-deficient mice. **J Cell Biol** (2005)

Katsuyama Y, Okada T, Matsumoto J, Ohtsuka Y, Terashima T, Okamura, Y. Early specification of ascidian larval motor neurons. **Developmental Biology**(2005)

Brown E R, Nishino A, Meinertzhagen I A, Bone Q, Okamura Y. GABAergic synaptic transmission modulates swimming in the ascidian larva. **European Journal of Neuroscience** (2005)

本研究成果として、Journal of Neurophysiology に発表された論文のコピーを添付。

Articles in PresS. J Neurophysiol (June 14, 2006). doi:10.1152/jn.01264.2005

Ankyrin-G regulates inactivation gating of the neuronal sodium channel, Nav1.6

Emi Shirahata[1], Hirohide Iwasaki[2,3,4], Masahiro Takagi[2,3], Changqing Lin[1], Vann Bennett[5], Yasushi Okamura[2,3,4] & Kiyoshi Hayasaka[1]

[1]Department of Pediatrics, Yamagata University School of Medicine, 2-2-2 Iida-nishi, 990-9585 Yamagata, Japan

[2]Section of Developmental Neurophysiology, Okazaki Institute for Integrative Bioscience, Higashiyama 5-1, Myodaiji-cho, Okazaki, 444-8787 Aichi, Japan

[3]National Institute for Physiological Science, Myodaiji-cho, Okazaki, 444-8787 Aichi, Japan

[4]School of Life Science, Graduate University for Advanced Studies, Myodaiji-cho, Okazaki, 444-8787 Aichi, Japan

[5]Howard Hughes Medical Institute and Department of Cell Biology, Duke University Medical Center, Durham, NC 27710, USA.

Running head: Ankyrin-G reduces persistent sodium current of human Nav1.6 channel

Contact information:

Yasushi Okamura

Section of Developmental Neurophysiology, Okazaki Institute for Integrative Bioscience, Higashiyama 5-1, Myodaiji-cho, Okazaki, Aichi 444-8787, Japan.

Phone 81-564-59-5256, FAX 81-564-59-5259

email: yokamura@nips.ac.jp

Abstract: Ankyrin-G, a modular protein, plays a critical role in clustering voltage-gated sodium channels (Nav channels) in nodes of Ranvier and initial segments of mammalian neurons. However, direct effects of ankyrin-G on electrophysiological properties of Nav channels remain elusive. In this study, we explored whether ankyrin-G has a role in modifying gating properties of the neuronal Nav1.6 channel that is predominantly localized at nodes of Ranvier and initial segments. TsA201 cells transfected with the human Nav1.6 cDNA alone exhibited significant persistent sodium current (Ina-p). On the other hand, Ina-p was barely detected upon co-expression with ankyrin-G. Ankyrin-B, another ankyrin, did not show such an effect. Expression of chimeras between the two isoforms of ankyrin suggests that the membrane-binding domain of ankyrin-G is critical for reducing the Ina-p of Nav1.6. These results suggest that ankyrin-G regulates neuronal excitability not only through clustering Nav channels but also by directly modifying their channel gating.

Key words

Ankyrin, sodium channel, inactivation gating

Introduction

Ankyrins are the multidomain adaptor proteins that link the spectrin/actin network to the cytoplasmic domain of membrane proteins, including ion channels and cell adhesion molecules (Bennett 1992) (Bennett and Gilligan 1993). Ankyrins consist of three major domains; a membrane-binding domain with a similar folding structure and the 24 consecutive repeats (the MB domain), a spectrin-binding domain (the S domain) and a death domain with the C-terminus (the DC domain) (Bennett and Baines 2001). Among three ankyrin isoforms, ankyrin-G is expressed abundantly at the axon initial segment and nodes in myelinated axons and directly interacts with axonal Nav channels (Bennett and Baines 2001; Kordeli et al. 1995). Ankyrin-G is known to play an essential role in rapid saltatory conduction of myelinated axons: in knock out mice of ankyrin-G, Nav channels are absent from axon initial segments and the nodes of Ranvier, and neurons of these mice show severe deficits in action potential firing (Zhou et al. 1998) (Jenkins and Bennett 2001).

Recently, in the human Nav1.5 sodium channel, a mutation in the consensus sequence for binding to ankyrin-G has been reported to be associated with Brugada syndrome, a dominantly inherited cardiac arrhythmia (Mohler et al. 2004b). This mutation drastically reduces surface expression of Nav1.5 channel in cardiomyocytes. In addition, heterologous expression of this mutant hNav1.5 channel showed distinct gating behavior compared to the wild-type channel. This suggests that ankyrin-G may have a modulatory effect on gating properties of sodium channel besides clustering or recruitment of Nav channels to the cell membrane.

In the present study, we aimed to explore the regulatory role of ankyrin-G in gating properties of a neuronal sodium channel, Nav1.6, which predominantly expresses at the nodes of Ranvier and the initial segment(Caldwell et al. 2000). cDNA encoding hNav1.6 was transfected into tsA201 cells which do not express endogenous ankyrin. We show that ankyrin-G negatively regulates persistent sodium current (Ina-p) through the hNav1.6 channel. This raises the possibility that ankyrin-G regulates neuronal excitability not only through clustering Nav channels, but also through modifying gating behaviors of Nav1.6 channels.

Materials and Methods

cDNA preparation and transfection

Human Nav1.6 cDNA was isolated from a lamda gt11 human spinal cord cDNA library, which contained a 5940-bp open reading frame (NCBI AB027567). The T4910C mutation was corrected and the cDNA fragment containing the adult type of exon 5 was used to construct a full length cDNA in pUC19. For expression in tsA201 cells, a CMV promoter from the pcDNA3 vector (Invitrogen) was subcloned upstream of the coding region of Nav1.6 in hNav1.6-pUC19 (CMV-hNav1.6-pUC19). 270 kDa ankyrin-G and 220 kDa ankyrin-B were expressed as fusion proteins with enhanced green fluorescent protein (GFP) at the N-terminus. Ankyrin-B/G chimeras contain GFP at the C-terminus(Mohler et al. 2002).

TsA201 cells were transiently transfected with SuperFect or PolyFect (QIAGEN) according to the manufacturer's protocols and cultured for 30-72 hrs. To express Nav channels consisting only of alpha-subunit protein, cells were transfected with CMV-hNav1.6-pUC19 and pEGFP-C1 (BD Biosciences). For coexpression with rat sodium channel beta1 subunit (Navβ1), Nav1.6 cDNA was cotransfected with the plasmid of pCD8-IRES-β1, containing a pCD8 coding region, in tandem with the Navβ1-coding region, and transfected cells were identified by labeling with anti-CD8 coated beads (DYNAL M-450 CD8).

Electrophysiology

Electrophysiological recordings of tsA201 cells were performed at room temperature with whole cell patch clamp techniques using an EPC-9 amplifier (HEKA Electronik, Germany). The extracellular solution consisted of 150 mM NaCl, 2 mM KCl, 1.5 mM $CaCl_2$, 1 mM $MgCl_2$, 10 mM glucose and 10 mM 4-(2-hydroxethel)1- piperazine-ethanesulphanic acid (HEPES), pH7.4. The internal pipette solution consisted of 117 mM CsCl, 9 mM ethylene glycol-bis (β-amino-ethyl ether) N,N,N',N'-tetra acetic acid (EGTA), 9 mM HEPES, 1.8 mM $MgCl_2$, 14 mM Tris-creatine PO_4, 4 mM Mg-ATP and 0.3 mM Tris-GTP, pH 7.4. Pipettes of resistance 1.8-3.5 Mohms were used. We noted that Ina-p was highly sensitive to the composition of the internal solution; little Ina-p was observed when CsF instead of CsCl was used, as previously reported (Burbidge et al. 2002). Junction potentials (–2 mV on average) were not compensated. In cells with current amplitude over 1 nA, series resistance was compensated up to 80%. No untransfected cell exhibited the peak amplitude of inward sodium currents over 100 pA. TTX subtraction experiments were performed with a fast perfusion system using the DAD12-system (ALA scientific). The current-voltage relationship was analyzed via a step protocol in which cells were depolarized from a holding potential of -80 mV. Each interval was 5 sec and leakage currents were subtracted using the P/N method with N values ranging between 4 and 10. Ina-p was measured as steady-state inward currents at 100 ms for most data, and at 20 ms in data used in Fig.2, after the beginning of depolarization. The voltage dependence of steady-state inactivation was determined via a two-step protocol in which a 300 msec conditioning pulse was applied from a holding potential of –80 mV

followed immediately by a test pulse to 10 mV. Analysis was performed using PulseFit software (HEKA) and IgorPro (Wavemetrics). Results are presented as mean ± SE (standard error), and statistical significance was determined using an unpaired *t*-test.

Measurements of Ina-p

%pc was obtained by calculating the ratio of Ina-p against the maximum peak amplitude of transient inward currents in the series of step pulses. Current amplitudes were obtained by leak subtraction using the P over N protocol except in Fig.2. As seen in Figures (eg. Fig1,3), inward currents reach steady-state within 20 ms in most ranges of membrane potential. In order to minimize the error in estimating %pc, we utilized low sodium internal solution. The rationale described in Results section is based on the fact that Ina-p attains its maximum value around at +10 mV, more positive than the voltage that gives the peak amplitude of the fast inward component. In order to maximize the inward Ina-p, a solution with low sodium concentration was used in patch pipette throughout this study.

RT-PCR

Total RNA of tsA201 was isolated using Trizol reagent (Invitrogen) following the manufacturer's protocol. cDNA was synthesized using Superscript (Invitrogen) primed with oligo-dT. For DNA amplification of human ankyrin-G, -B, -R, PCR primers were designed in two distinct regions: the ankyrin-repeat region and the

spectrin binding domain. Sequences were selected such that they could discriminate among three isoform genes. Both sets of primers gave similar results. The following oligonucleotides correspond to the spectrin-binding domain: ank-G-forward (CACAGACAAATATCTTGGG) and ank-G-reverse (TCTAAGAGAATCTGAATCAA) for ankyrin-G, ank-B-forward (GCCTGAGGACCTAAAAGAAC) and ank-B-reverse (CCCCAGCTTAGGCGATAAGC) for ankyrin-B, ank-R-forward (GATGAAGGGGAAGAACTCATC) and ank-R-reverse (TGTCTGAGGTCTCGGTGGCC) for ankyrin-R, respectively. Primers corresponding to the ankyrin-repeat domain were: ankG-Repeat-F (GATCATTTAAACTGCGTCCAG) and ankG-Repeat-R(CCATGATGCATTAGTTGTGA) for ankyrin-G, ankB-Repeat-F(GACCACGTGGAATGTGTGAA) and ankB-Repeat-R(GGCTCCGTTCTGCAGCAGAAG) for ankyrin-B, ankR-Repeat-F(GACCACCTCGACTGTGTCCGG) and ankR-Repeat-R(CCCCGCTGCAGGAGGTTCTT) for ankyrin-R, respectively. PCR reaction was performed under the condition:28 cycles of 94 °C for 50 seconds, 54 degree for 60 °C, 72 °C for 60 seconds. As positive control, cDNA was synthesized from human adult brain RNA (purchased from BD Bioscience), and amplified with the same sets of primers as in the cDNA from tsA201 cells.

Results

Human Nav1.6 sodium channels expressed in tsA201 cellsshow robust Ina -p

hNav1.6 plasmid was transfected into tsA201 cells for whole cell patch recording. The full-length hNav1.6 protein by this plasmid was confirmed by the expression of a protein about 250 kd in molecular size following transfection into COS1 cells as detected by western blot (Supplementary figure 1) with the monoclonal anti-pan sodium channel antibody (courtesy of Dr. James Trimmer). Inward currents recorded from tsA201 cells transfected with hNav1.6 consisted of a rapid, transient component (peak current) and a sustained component that persisted even after pulses of 100 ms (persistent current; Ina-p) (Fig 1), consistent with a previous report (Burbidge et al. 2002). A marked amount of Ina-p was observed in most cells (10.5±1.8% at +10 mV) (*n*=7) (Fig 1B). The current-voltage relationship (I-V curve) (Fig. 1C) for both peak current and the persistent component showed that Ina-p reached the maximum amplitude at a more positive voltage than the transient current; the Ina-p attained its peak at +10 mV, whereas the transient current did so at 0 mV. Such a difference in the peak voltage between the fast transient current and the Ina-p was also noted in *Xenopus* oocytes (data not shown), consistent with a previous study (Smith et al. 1998).

The steady-state inactivation curve of Nav1.6 currents showed a shoulder around at –50 to –30 mV and two components of the Boltzmann equation were needed to fit the data (Fig 1D) (the two half inactivation voltages, $V_{1/2a}$, $V_{1/2a}$, for Nav1.6 are –61.9±1.1 mV and –22.5±2.1 mV with slopes of 9.6±2.2 and 7.8±4.3 (*n*=6), respectively). The transient peak current decreased as conditioning pulses became

more positive. In contrast, the slow component was more resistant to conditioning pulse up to +10 mV (see non-zero value over +10 mV in Fig 1D and inset trace). To clarify whether robust Ina-p is a feature unique to Nav1.6, another neuronal sodium channel, rat Nav1.2 (rNav1.2), was also recorded. The peak sodium current of Nav1.2 was 90.0±8.9 pA/pF (*n*=4). Ina-p was significantly smaller in Nav1.2-transfected cells than that in Nav1.6-transfected cells (2.5±0.5% (*n*=3) at 0 mV for Nav1.2). In contrast with the biphasic profile in Nav1.6-transfected cells, Nav1.2-transfected cells exhibited a simple profile of the steady-state inactivation curve which could be fitted by a single Boltzmann equation (Fig. 1D)($V_{1/2}$ –53.8 mV and a slope of 6.0). We also recorded hNav1.1 and hNav1.5 under the same conditions and observed much less Ina-p compared with the hNav1.6 channel (data not shown).

Quantification of Ina-p could be affected by the presence of some endogeneous currents, in particular, at high depolarizing levels. To verify the method of estimation of Ina-p with the P/N protocol, the Nav channel currents were compared between the TTX-subtraction method (Fig. 2A) and the P/N protocol in the same cells. Fig. 2B indicates a typical example of superimposed traces between the TTX-subtraction method (blue) and P/N protocol (red) from the same cell. The persistent component does not significantly differ between the two protocols over a wide range of membrane potential lower than 20 mV. This was also supported by the plots from accumulated data from 9 cells (Fig. 2C). However, the transient inward current with TTX-subtraction slightly deviates from that with the P/N protocol at higher depolarizations (Fig. 2B, +20 mV, +30 mV). This is probably because the kinetics of

the inward current are faster at higher depolarizations and more readily subject to errors due to fluctuating capacitative currents. Therefore, in the following experiments with P/N protocol, we quantified the proportion of Ina-p over a range of membrane potentials, including 0 mV to +10 mV. The peak amplitude of transient current with P/N protocol tended to be smaller than that with TTX-subtraction at higher voltages, probably because more uncancelled capacitative currents overlapped with the transient sodium currents that become sharper as the membrane potential is more depolarized. The proportion of Ina-p at each membrane potential was therefore measured by standardizing Ina-p with the maximum peak of the transient inward current in the I-V curve (termed %pc) in later experiments. We also checked the quality of voltage clamp condition by comparing the I-V curve between the two external solutions, containing 150 mM and 50 mM sodium ions. Fig. 2D shows a typical example of such data. The I-V curve does not significantly change between the two conditions. Similar results were obtained from other four cells. Therefore, it is unlikely in our measurements that imperfect voltage clamp causes error of estimation of %pc.

Several mammalian Nav channels are known to exhibit the slowly inactivating component in *Xenopus* oocyte which is normalized by the coexpression of sodium channel β1-subunit (Wallner et al. 1993). To test if inactivation gating of hNav1.6-derived currents depend on the auxiliary subunit, β1-subunit was coexpressed with hNav1.6. Coexpression with β1-subunit did not significantly increase the Nav current densities (51.2±1.1 pA/pF (n=30) and 87.9±12.2 pA/pF (n=6) for cells expressing Nav1.6 alone and Nav1.6 plus β1, respectively) (Fig. 3). No significant

difference in the %pc was found between transfection of Nav1.6 with the β1-subunit and that of Nav1.6 alone (Fig 3D) (10.8±0.7% at +10 mV (*n*=7) for Nav1.6 alone; 12.8±0.5% (*n*=4) for Nav1.6+β1). The steady-state inactivation curve was shifted to a slightly more negative potential (Fig 3E). The activation kinetics were compared by measuring the rising time to half of the peak amplitude ($t_{1/2}$) (Fig.4). The $t_{1/2}$ (647±37 μs (*n*=5)) was significantly faster than that of cells without the β1-subunit (912±54 μs (*n*=13), respectively). A shift in steady-state inactivation and faster rising time verify that the β1-subunit was functionally expressed.

Coexpression of Ankyrin-G decreases the Ina-p of hNav1.6

Before testing the role of ankyrin-G in regulating Nav channel gating properties, we first examined whether tsA201 cells express endogenous ankyrin-G or ankyrin-B. RT-PCR was performed with primers each specific to human ankyrin-G and –B (Fig. 5). Both primers gave positive bands from brain cDNA, whereas no signal was obtained for either isoform of ankyrin with cDNA from tsA201 cells. Actin primers as positive control gave signals under the same conditions. The third ankyrin isoform, ankyrin-R, was also tested and found not expressed (data not shown). We therefore concluded that tsA201 cells will provide an appropriate model to test the role of heterologously expressed ankyrin on Nav channels.

Effects of ankyrin-G on hNav1.6 were tested both in the absence or presence of β1-subunit. Coexpression with ankyrin-G did not increase peak inward currents in a statistically significant manner (51.2±1.1 pA/pF (*n*=30) for Nav1.6 alone, and

45.3±0.85 pA/pF (*n*=28) for Nav1.6 plus ankyrin-G, respectively). Peak sodium curents of cells expressing Nav1.6 plus ankyrin-G and β1 (78.3±14.9 pA/pF (*n*=4)) were slightly larger than those of cells expressing Nav1.6 alone or Nav1.6 plus ankyrin-G. Importantly, the coexpression with ankyrin-G significantly reduced Ina-p (3.6±0.3% at –10 mV (*n*=6) for Nav1.6+ankyrin-G; 3.8±1.2% at 0 mV (*n*=3) for Nav1.6+ankyrin-G+β1 vs 10.8±0.7% at +10 mV (*n*=7) for Nav1.6 alone) (Fig. 3B, C, D). Such a reduction in Ina-p by ankyrin-G was also reflected in the steady-state inactivation curve, which did not show the shoulder at higher voltage (depolarization ranging from -50 mV to +10 mV) (Fig. 3E). In addition, cells expressing ankyrin-G showed a small non-inactivating component at +10 mV and the inactivation curves were fitted by a single Boltzmann equation ($V_{1/2}$ and slopes were –50.4±2.8 mV and 15.7±3.1 (*n*=6) for Nav1.6 plus ankyrin-G, and –54.6±1.7 mV with and 9.6±0.8 (*n*=3) for Nav1.6 plus ankyrin-G and β1, respectively). I-V curves were shifted by about 8 mV leftward in cells transfected with Nav1.6 and ankyrin-G (Fig. 3C). However, ankyrin-G did not show a significant effect on activation kinetics; the $t_{1/2}$ of Nav1.6 alone, Nav1.6 plus ankyrin-G, and Nav1.6 plus ankyrin-G plus β1 were 912±54 μs (*n*=13), 789±50 μs (*n*=13), and 611±52 μs (*n*=4), respectively (Fig. 4).

Membrane-binding domain of ankyrin-G is critical for reduction of hNav1.6-derived Ina-p

We tested whether ankyrin-B, another isoform of ankyrin abundantly expressed in mammalian neurons (Kunimoto et al. 1991), also shows the modulation activity of

Nav1.6 inactivation. Maximum peak amplitudes of hNav1.6 coexpressed with ankyrin-B were 51.3±5.7 pA/pF (*n*=9), which did not show significant difference against that of hNav1.6 alone or hNav1.6 with ankyrin-G. The Ina-p of hNav1.6 did not decrease on coexpression with ankyrin-B (Fig. 6B). The %pc of the cell coexpresssing hNav1.6 with ankyrin-B was as large as that of hNav1.6 alone (12.1±1.1% at 0 mV (*n*=4) for hNav1.6+ankyrin-B; 10.8±0.7% at +10mV (*n*=7) for hNav1.6 alone)(Fig 6D). The steady-state inactivation curve showed a shoulder around –50 to –30 mV and two components of the Boltzmann equation were needed to fit the data (Fig 6E) ($V_{1/2a}$, $V_{1/2a}$ –65.6±1.9 mV and –17.1±3.9 mV, with slopes of 5.1±1.2 and 7.7±1.6 (*n*=5)) as in cells only transfected with hNav1.6 cDNA. I-V curves observed from cells expressing ankyrin-B were similar to those of cells with Nav1.6 alone (Fig. 6C).

To define a region within ankyrin-G that confers modifying ability for inactivation of hNav1.6, we expressed hNav1.6 with five distinct chimeras between ankyrin-G and B (Mohler et al. 2002) (Fig. 7A). Expression of ankyrin chimera was confirmed by the fluorescent signal of GFP which was fused at the N-terminus of each chimeric protein. In the cells expressing the protein which contained the MB domain of ankyrin-B, %pc was as the same thatof cells expressing hNav1.6 alone (Fig 6B, C, Table1). In contrast, all chimeras that contained the ankyrin-G MB domain showed small %pc (Fig 7D, Table1). These findings suggest that the MB domain of the ankyrin-G is critical for the reduction of Ina-p of hNav1.6. This also supports the idea that reduction of Ina-p by ankyrin-G is mediated by direct binding to hNav1.6.

To confirm that physical association of ankyrin-G with hNav1.6 underlies the reduction of Ina-p, we tried experiments of immunocoprecipitation using antibodies against ankyrin-G and hNav1.6. However, we failed to detect this interaction, although pan-sodium channel antibody detected a faint but clear band in the immunoblot of heterologously expressed hNav1.6 (supplementary figure 1). Our failure to detect direct binding of hNav1.6 with ankyrin-G in immunocoprecipitation experiment was probably due to the low level of expression of hNav1.6 in our system. The cytoplasmic linker of the sodium channel alpha subunit was known to associate with the membrane domain of ankyrin-G. A target motif in cytoplasmic II-III linker has been identified as a critical reigon that is sufficient to localize membrane proteins at the axon initial segment by a process involving association with ankyrin-G (Garrido et al. 2003) (Lemaillet et al. 2003). To test if this region is required for correction of inactivation gating by ankyrin-G, Nav1.6 lacking the target motif (VPIAVGESD, V1092_D1100, Nav1.6ΔII-III) was constructed and transfected into tsA201 cells. However, Ina-p of this construct was significantly smaller than that of wild-type Nav1.6 (6.6+4.6% at 0 mV (n=6) for Nav1.6ΔII-III; 10.5+4.8% at 10 mV (n=7) for Nav1.6 alone). This could probably be due to the direct affect of deletion of the 9 amino acid motif on gating properties. Therefore we were not able to test the direct binding of hNav1.6 to ankyrin-G using this construct.

As alternative approach, GFP-fused ankyrin-G was visualized under confocal microscope following cotransfection with hNav1.6 cDNA. GFP signals were located mainly on the periphery of cells or borders between cells, probably reflecting that

ankyrin-G is recruited to cell membrane with hNav1.6 (Fig. 8). This pattern depended on the presence of hNav1.6, since GFP signal was equally distributed in the cytoplasm when GFP-fused ankyrin-G alone was expressed or GFP-fused ankyrin-B was coexpressed with hNav1.6.

Discussion

We examined the potential roles of ankyrin-G, an adaptor protein enriched at the node of Ranvier, on gating properties of hNav1.6 channels in tsA201 cells. We found that ankyrin-G significantly reduces Ina-p of hNav1.6 channels.

Estimation of Ina-p of the Nav1.6 channel

In some cases with large current densities of Nav currents, estimation of %pc may not be accurate due to imperfectly controlled voltage clamp condition. To verify voltage clamp condition, we compared I-V curve under the two conditions, 50 mM sodium solution and 150 mM sodium solution (Fig. 2D). Results showed that I-V curve does not significantly shift between the two conditions in all cells showing less than 1 nA of peak inward currents, suggesting that peak currents are measured under well-controlled voltage clamp conditions. However, in cells showing more than 1 nA (corresponding to the current density, about 200 pA/pF), I-V curve was slightly shifted leftward. In this study, some cells exhibited the current density over 200 pA/pF. This potentially causes some error in estimation of %pc. Due to such potential inaccuracy

of estimation of %pc, we should be cautious about the absolute value of %pc in our study. However, it is unlikely that this affects significance of the difference of %pc obtained between the two groups which is three times larger in our study, since only a small number of cells showed current amplitudes over 1 nA.

Cells transfected with hNav1.6 cDNA showed robust Ina-p, consistent with previous expression studies in *Xenopus* oocytes (Smith et al. 1998) and HEK293 cells (Burbidge et al. 2002). On the other hand, in recent experiments of forced expression of Nav1.6 into cultured DRG neurons, which were engineered to be TTX-resistant by single point mutation, Nav1.6-derived currents did not exhibit robust Ina-p (Herzog et al. 2003). This discrepancy could be in part due to different conditions of electrical recording or cell preparation. In particular, Ina-p could be highly sensitive to the composition of the internal solution. In the previous work (Herzog et al. 2003), CsF was utilized in an internal solution. We observed that Ina-p was significantly smaller in hNav1.6-transfected tsA201 cells with CsF in the internal solution instead of CsCl, as also reported previously (Burbidge et al. 2002).

On coexpression of ankyrin-G, the steady-state inactivation curve was shifted leftward in accordance with the reduction in Ina-p. This shift did not occur equally over the entire range of membrane potential, but was more remarkable at a less negative region. This is consistent with the idea that the persistent component of Nav1.6-currents in the present study may reflect a channel population that fails to inactivate. However, this does not neglect the possibility that some component of Ina-p by Nav1.6 is due to the “window current”, which has been suggested as one of the

underlying mechanisms of Ina-p in CNS neurons (Taddese and Bean, 2002), or due to a modal change in the transition into a bursting mode of channel function (Patton et al. 1994).

We should note that some characteristics of Ina-p observed in tsA201 cells are slightly different from those reported in native neurons. In the experiments on heterologous expression, the peak voltage of Ina-p was shifted to a more positive region of the membrane potential, compared with that of the transient current (Smith et al. 1998) (Fig. 1). In some native neurons (Kay et al. 1998; Magistretti and Alonso 1999), however, Ina-p is largest at a more negative membrane potential than the voltage that gives the maximum transient current. In native neurons, Nav channels usually consist of multiple molecular species of the alpha subunits (Chahine et al. 2005). It is possible that the underlying mechanisms for Ina-p could be diverse among Nav channel isoforms and the behaviors of Ina-p of the Nav1.6 channel in heterologous expression may reflect a restricted population of Nav channels underlying Ina-p observed in native neurons.

Modulation mechanisms of Nav1.6-derived Ina-p by ankyrin-G

In this study, we failed to provide direct evidence that hNav1.6 directly binds to ankyrin-G in our experimental system despite several trials of immuno-coprecipitation experiments. Ankyrin is known to interact with spectrins that associate with the actin cytoskeleton (Bennett and Baines 2001). In several reports (Shcherbatko et al. 1999), the inactivation kinetics of sodium channels significantly changes when membrane associated cytoskeleton is disrupted. This suggests that inactivation gating of sodium

channels depends on membrane associated cytoskeleton. In our recording under the perforated patch configuration without applying negative pressure (data not shown), we observed robust Ina-p in cells only expressing Nav1.6 and reduced Ina-p in cells coexpressing ankyrin-G. It is unlikely that ankyrin-G modulates sodium channel gating through indirect mechanisms such as global perturbation of the cytoskeleton or change of cellular morphology. In fact, ankyrin-B, which has actin-recruiting activity, did not exhibit Ina-p reduction. Experiments using chimeras between ankyrin-G and -B suggest that the MB-domain confers isoform-specific inhibition of Ina-p, supporting the idea that direct binding of ankyrin proteins to Nav1.6 mediates modulation of Ina-p. Ankyrin specificities have been described for interactions between IP3 receptors and ankyrin-B in cardiac muscle cells (Mohler et al. 2004a). Ankryin G did not rescue mislocalization of IP3 receptors in cardiac muscle cells in ankyrin-B knockout mice (Mohler et al. 2002). From transfection experiments of various chimeras between ankyrin-G and ankyrin-B, the specificity of the interaction with IP3 receptors between ankyrin-B and ankyrin-G has been assigned to the C-terminal regulatory domain but not to the N-terminal binding domain (Mohler et al. 2002). We do not know the reason for such discrepancy of the specificity of ankyrin isoforms between our study and studies on cardiac cells.

One possible biophysical mechanism of suppression of Ina-p by ankyrin-G may be that two populations of Nav1.6 channels with distinct inactivation properties coexist and ankyrin-G may reduce the number of channels that fail to inactivate. Alternatively, ankyrin-G may uniformly affect the whole population of sodium channels and allow

channels to more readily adopt a mode in which channels faithfully inactivate by the fast inactivation mechanism. In either case, the amplitude of peak sodium current might be slightly reduced compared to cells expressing only hNav1.6. However, we were not able to detect any significant effect of ankyrin-G on the current density. It is possible that a minor decrease of the current amplitude by ankyrin-G was within the variability of the current density among cells, or that slight enhancement of recruitment of Nav1.6 proteins on the cell membrane by ankyrin-G might have balanced the slight reduction of the current amplitude.

It is possible that binding of ankyrin-G changes the local structure of the cytoplasmic domains of hNav1.6 protein, thereby modulating inactivation gating. Recent studies have identified the critical consensus motif, consisting of 9 amino acids, in the II-III cytoplasmic loop of Nav channels, that binds to the MB-domain of ankyrin-G and mediates clustering of Nav channels at the node of Ranvier and initial segment (Garrido et al. 2003; Lemaillet et al. 2003). Mutation in the II-III loop has been reported to affect inactivation gating of Nav channels (Kuzmenkin et al. 2003). In addition, ankyrin is known to physically bind to the III-IV linker (Bouzidi et al. 2002) that plays a critical role in inactivation gating. On the other hand, lna-p significantly decreases after long whole cell recordings and Ina-p is rarely observed when CsF was utilized as the pipette solution. It is therefore possible that Ina-p is sensitive to the cellular metabolic state, for example, through some state of phosphorylation of the cytoplasmic regions of the Nav1.6 channels. Ankyrin-G, a large globular protein, may sterically affect such phosphorylation of Nav1.6 channel

proteins. Understanding the mechanisms of modulation of inactivation by ankyrin-G must await further studies such as single channel recording and biochemical studies.

Possible physiological and pathophysiological implications of "ankyrin-G-dependent gating" of Nav1.6 channels

Functional diversity of Nav channels underlies the complexity of mammalian neuron excitability that include integration, pacemaking and conduction. Ina-p has been reported to be present in cell soma (Kay et al. 1998) and dendrites (Magistretti et al. 1999). Nav1.6 knockout mice show less Ina-p in accordance with fewer spontaneous firings (Raman et al. 1997), indicating that Nav1.6 is the major contributor of neuronal Ina-p. On the other hand, Nav1.6 is the predominant axonal sodium channel. Robust Ina-p of Nav1.6 has been reported in experiments with heterologous cells, including *Xenopus* oocytes (Goldin 1999) and HEK293 cells (Burbidge et al. 2002). In the present study, expression of ankyrin-G rendered the Nav1.6 current more completely inactivated such that Nav currents resembled those of the mammalian node (Schwarz et al. 1995). These findings raise the possibility that Ina-p could be the default state property of Nav1.6 channels, and that the amplitude of Ina-p is suppressed through interaction with ankyrin-G protein at the node of Ranvier. Ankyrin-dependent inhibition of Ina-p at the node of Ranvier may play a role in ensuring generation of individual action potentials following single action potentials that propagate from the upstream node. On the other hand, in the cell soma, Ina-p based on Nav1.6 escapes inhibition by ankyrin-G, probably because ankyrin-G expression is extremely low in the

cell soma (Kordeli et al. 1995). Interaction of Nav1.6 channels with ankyrin-G may be one of the molecular bases for the functional diversity of Nav channels in neurons.

If ankyrin-G regulates inactivation gating of *in vivo* axons, inactivation behaviors of nodal Nav channels may change under some pathological conditions such as demyelination. Abnormal axonal excitations arising spontaneously, and frequently firing, are known to be observed in demyelinating conditions, such as in multiple sclerosis (Smith and Hall 2001) or after nerve injury (Sommer 2003). In multiple sclerosis patients, as well as in experimental autoimmune encephalomyelitis (EAE), a mouse model of multiple sclerosis, a Na-Ca exchanger is colocalized with Nav1.6 along the demyelinated nerve (Craner et al. 2004). Increased sodium influx through Nav1.6 has been proposed to cause an increase in intracellular calcium concentration by activating the Na-Ca exchanger (Craner et al. 2004). Demyelination and nerve injury may down-regulate ankyrin-G at the node, leaving a population of Nav1.6 in the membrane. This may lead to disinhibition of Ina-p, increasing sodium influx. This idea could be tested by examination of expression patterns of Nav1.6 and ankyrin-G in such demyelinating nerves.

Acknowledgements

We thank Dr. J. Trimmer for providing pan-sodium channel antibody, K58/35.4, and help in immunoblot experiment in COS1 cells, Dr. M. Chahine for critical reading of the manuscript and providing the rat sodium channel β1 subunit, Dr. K. Imoto and Dr. M. Noda for providing rat brain Nav1.2 clones, Dr. Alan Goldin for providing mouse

SCN8a plasmid that was used in early phase of this study, Dr. Izumi-Nakaseko for exchanging preliminary results of mouse Nav1.6 channel in HEK293 cells, M. Sasaki for help in RT-PCR and Dr. T. McCormack for reading the manuscript. Accession number for the full-length human Nav1.6 is NCBI AB027567.

Grants

This work was supported by Grants in Aids for Scientific Research to K. H. and Y. O.

Figure Legends

Fig. 1. Whole cell Nav currents recorded from tsA201 cells transfected either with hNav1.6 or the rNav1.2 α-subunit. (A, B) Representative traces were elicited by membrane depolarizations for 100 ms ranging from –30 to +50 mV in 10 mV increments from a holding potential of -80 mV. The same trace in (A) is expanded in (B) at a different time scale. The peak sodium curents of hNav1.6 and rNav1.2 were 51.2±1.1 pA/pF (*n*=30) and 90.0±8.9 pA/pF (*n*=4), respectively. (C) The current-voltage relationship (I-V curves) of hNav1.6 (○) and rNav1.2 (*). Values were normalized by the maximum amplitude. (D) The voltage dependence of steady-state inactivation and representative traces (insets) for hNav1.6 and rNav1.2. Representative traces with a preconditioning pulse to –110 mV (dotted lines) and –20 mV (solid lines) indicate that the rNav1.2 channel was completely inactivated by a conditioning pulse to –20 mV.

Fig. 2. Comparison of inward currents of hNav1.6 between a TTX-sensitive inward current versus a current measured with P/N protocol. A. An example of raw traces before (black) and after (red) application of TTX. Capacitative current and leakage are not corrected. B. Representative traces from one cell at different membrane potentials. Blue indicates the trace obtained with TTX-subtraction and red indicates that with the P/10 protocol. C. X-Y plot of current amplitudes of Ina-p obtained with P/10 and TTX-subtraction from eight cells expressing hNav1.6 cDNA. Data of 0 mV, +10 mV, +20 mV were from 9 cells. Data of 30 mV was from 8 cells. D. The I-V curve of

transient inward currents compared under 150 mM sodium and 50 mM sodium. In the lower plot, current amplitude was normalized by the peak value.

Fig. 3. Whole cell sodium currents recorded from tsA201 cells expressing the hNav1.6 α-subunit alone or with ankyrin-G (AnkG) or/and β1-subunit. (A, B) Maximum amplitudes of sodium currents from cells expressing hNav1.6 alone, hNav1.6+AnkG, hNav1.6+β1, and hNav1.6+AnkG+β1 were 51.2±1.1 pA/pF (*n*=30), 45.3±0.85 pA/pF (*n*=28), 87.9±12.2 pA/pF (*n*=6), 78.3±14.9 pA/pF (*n*=4), respectively. The same records in (A) are shown in a different time scale in (B). (C) The I-V curves obtained from cells transfected with Nav1.6 alone (○), hNav1.6+AnkG(□), hNav1.6+β1 (●), or hNav1.6+β1+AnkG (■). (D) Voltage dependence of the proportion of Ina-p (%pc). Without AnkG, %pc was larger (*; $p<0.05$, **; $p<0.01$). (E) The steady-state inactivation curve. Current traces during the test stimuli are shown (the upper panel). The curve of cells expressing AnkG was fitted with a single Boltzmann equation.

Fig. 4. Rising time to half the peak amplitude ($t_{1/2}$) was determined for cells expressing hNav1.6 alone and cells coexpressing Nav1.6 with ankyrin-G and/or the sodium channel β1-subunit. The $t_{1/2}$ of hNav1.6 alone (○), hNav1.6 plus ankyrin-G (□), hNav1.6 plus β1 (●), and hNav1.6 plus ankyrin-G plus β1 (■) were 912±54 μs (*n*=13), 789±50 μs (*n*=13), 647±37 μs (*n*=5), and 611±52 μs (*n*=4), respectively. Asterisks indicate significant difference.

Fig. 5. RT-PCR shows no endogenous expression of ankyrin-G or -B gene in tsA201 cells. Right two lanes denote no signal from tsA201 cDNA, but the third and fourth lane shows clear positive signals from brain cDNA. Integritiy of cDNA was checked by the expression of actin (right lane).

Fig. 6. Distinct effect between ankyrin-G (AnkG) and ankyrin-B (AnkB) on the Ina-p of the hNav1.6 channel. (A,B) Representative traces are shown with distinct time scale. Maximum current densities of Nav channel currents from cells expressing hNav1.6 alone, hNav1.6+AnkG, and hNav1.6+AnkB were 51.2±1.1 pA/pF (n=30), 45.3±0.85 pA/pF (n=28) 51.3±5.7 pA/pF (n=9), respectively. (C) The I-V curves from cells expressing hNav1.6 alone, hNav1.6 and AnkB (♦) and hNav1.6 and AnkG (□). (D) %pc at different membrane potentials (*; $p<0.05$, **; $p<0.01$) (E) The steady-state inactivation curve. Current traces during the test stimuli are shown (the upper panel). Fitting the curve from cells coexpressing with AnkB (▲)($n = 5$) required two components of the Boltzmann equation.

Fig. 7. Effect of coexpression of ankyrin-B/G chimeras on the Ina-p of Nav1.6. (A) The scheme of ankyrin-B/G chimeras. (B, C) Representative traces recorded from tsA201 cells expressing ankyrin-B/G chimeras. Maximum current densities of Nav channel currents were not significantly different among chimeras. (D) %pc at distinct membrane potentials.

Fig. 8. Localization of ankyrin protein analyzed by confocal microscopy. Cells were transfected with hNav1.6 and GFP-fused ankyrin-G. Note that signal is most abundant at the pheriphery of cells (middle panel), whereas signal was more diffuse when ankyrin-G alone or ankyrin-B was expressed.

Supplementary Figure 1. (in Supplementary data pdf file)

Western blot of hNav1.6 heterologously expressed in COS1 cells using the monoclonal antibody, K58/35.4, against the pan-sodium channel antigens.

References

Bennett V. Ankyrins. Adaptors between diverse plasma membrane proteins and the cytoplasm. *J Biol Chem* 267: 8703-8706, 1992.

Bennett V and Baines AJ. Spectrin and ankyrin-based pathways: metazoan inventions for integrating cells into tissues. *Physiol Rev* 81: 1353-1392, 2001.

Bennett V and Gilligan DM. The spectrin-based membrane skeleton and micron-scale organization of the plasma membrane. *Annu Rev Cell Biol* 9: 27-66, 1993.

Bouzidi M, Tricaud N, Giraud P, Kordeli E, Caillol G, Deleuze C, Couraud F, and Alcaraz G. Interaction of the Nav1.2a subunit of the voltage-dependent sodium channel with nodal ankyrinG. In vitro mapping of the interacting domains and association in synaptosomes. *J Biol Chem* 277: 28996-29004, 2002.

Burbidge SA, Dale TJ, Powell AJ, Whitaker WR, Xie XM, Romanos MA, and Clare JJ. Molecular cloning, distribution and functional analysis of the NA(V)1.6. Voltage-gated sodium channel from human brain. *Brain Res Mol Brain Res* 103: 80-90, 2002.

Caldwell JH, Schaller KL, Lasher RS, Peles E, and Levinson SR. Sodium channel Na(v)1.6 is localized at nodes of ranvier, dendrites, and synapses. *Proc Natl Acad Sci U S A* 97: 5616-5620, 2000.

Chahine M, Ziane R, Vijayaragavan K, and Okamura Y. Regulation of Na v channels in sensory neurons. *Trends Pharmacol Sci* 26: 496-502, 2005.

Craner MJ, Newcombe J, Black JA, Hartle C, Cuzner ML, and Waxman SG. Molecular changes in neurons in multiple sclerosis: altered axonal expression of Nav1.2 and Nav1.6 sodium channels and Na+/Ca2+ exchanger. *Proc Natl Acad Sci U S A* 101: 8168-8173, 2004.

Garrido JJ, Giraud P, Carlier E, Fernandes F, Moussif A, Fache MP, Debanne D, and Dargent B. A targeting motif involved in sodium channel clustering at the axonal initial segment. *Science* 300: 2091-2094, 2003.

Goldin AL. Diversity of mammalian voltage-gated sodium channels. *Ann N Y Acad Sci* 868: 38-50, 1999.

Herzog RI, Cummins TR, Ghassemi F, Dib-Hajj SD, and Waxman SG.

Distinct repriming and closed-state inactivation kinetics of Nav1.6 and Nav1.7 sodium channels in mouse spinal sensory neurons. *J Physiol* 551: 741-750, 2003.

Jenkins SM and Bennett V. Ankyrin-G coordinates assembly of the spectrin-based membrane skeleton, voltage-gated sodium channels, and L1 CAMs at Purkinje neuron initial segments. *J Cell Biol* 155: 739-746, 2001.

Kay AR, Sugimori M, and Llinas R. Kinetic and stochastic properties of a persistent sodium current in mature guinea pig cerebellar Purkinje cells. *J Neurophysiol* 80: 1167-1179, 1998.

Kordeli E, Lambert S, and Bennett V. AnkyrinG. A new ankyrin gene with neural-specific isoforms localized at the axonal initial segment and node of Ranvier. *J Biol Chem* 270: 2352 -2359, 1995.

Kunimoto M, Otto E, and Bennett V. A new 440-kD isoform is the major ankyrin in neonatal rat brain. *J Cell Biol* 115: 1319-1331, 1991.

Kuzmenkin A, Jurkat-Rott K, Lehmann-Horn F, and Mitrovic N. Impaired slow inactivation due to a polymorphism and substitutions of Ser-906 in the II-III loop of the human Nav1.4 channel. *Pflugers Arch* 447: 71-77, 2003.

Lemaillet G, Walker B, and Lambert S. Identification of a conserved ankyrin-binding motif in the family of sodium channel alpha subunits. *J Biol Chem* 278: 27333-27339, 2003.

Magistretti J and Alonso A. Biophysical properties and slow voltage-dependent inactivation of a sustained sodium current in entorhinal cortex layer-II principal neurons: a whole-cell and single-channel study. *J Gen Physiol* 114: 491-509, 1999.

Magistretti J, Ragsdale DS, and Alonso A. Direct demonstration of persistent Na+ channel activity in dendritic processes of mammalian cortical neurones. *J Physiol* 521 Pt 3: 629-636, 1999.

Mohler PJ, Gramolini AO, and Bennett V. The ankyrin-B C-terminal domain determines activity of ankyrin-B/G chimeras in rescue of abnormal inositol 1,4,5-trisphosphate and ryanodine receptor distribution in ankyrin-B (-/-) neonatal cardiomyocytes. *J Biol Chem* 277: 10599-10607, 2002.

Mohler PJ, Hoffman JA, Davis JQ, Abdi KM, Kim CR, Jones SK, Davis LH, Roberts KF, and Bennett V. Isoform specificity among ankyrins. An

amphipathic alpha-helix in the divergent regulatory domain of ankyrin-b interacts with the molecular co-chaperone Hdj1/Hsp40. *J Biol Chem* 279: 25798-25804, 2004a.

Mohler PJ, Rivolta I, Napolitano C, LeMaillet G, Lambert S, Priori SG, and Bennett V. Nav1.5 E1053K mutation causing Brugada syndrome blocks binding to ankyrin-G and expression of Nav1.5 on the surface of cardiomyocytes. *Proc Natl Acad Sci U S A* 101: 17533-17538, 2004b.

Patton DE, Isom LL, Catterall WA, and Goldin AL. The adult rat brain beta 1 subunit modifies activation and inactivation gating of multiple sodium channel alpha subunits. *J Biol Chem* 269: 17649-17655, 1994.

Raman IM, Sprunger LK, Meisler MH, and Bean BP. Altered subthreshold sodium currents and disrupted firing patterns in Purkinje neurons of Scn8a mutant mice. *Neuron* 19: 881-891, 1997.

Schwarz JR, Reid G, and Bostock H. Action potentials and membrane currents in the human node of Ranvier. *Pflugers Arch* 430: 283-292, 1995.

Shcherbatko A, Ono F, Mandel G, and Brehm P. Voltage-dependent sodium channel function is regulated through membrane mechanics. *Biophys J* 77: 1945-1959, 1999.

Smith KJ and Hall SM. Factors directly affecting impulse transmission in inflammatory demyelinating disease: recent advances in our understanding. *Curr Opin Neurol* 14: 289-298, 2001.

Smith MR, Smith RD, Plummer NW, Meisler MH, and Goldin AL. Functional analysis of the mouse Scn8a sodium channel. *J Neurosci* 18: 6093-6102, 1998.

Sommer C. Painful neuropathies. *Curr Opin Neurol* 16: 623-628, 2003.

Wallner M, Weigl L, Meera P, and Lotan I. Modulation of the skeletal muscle sodium channel alpha-subunit by the beta 1-subunit. *FEBS Lett* 336: 535-539, 1993.

Zhou D, Lambert S, Malen PL, Carpenter S, Boland LM, and Bennett V. AnkyrinG is required for clustering of voltage-gated Na channels at axon initial segments and for normal action potential firing. *J Cell Biol* 143: 1295-1304, 1998.

Figure 1

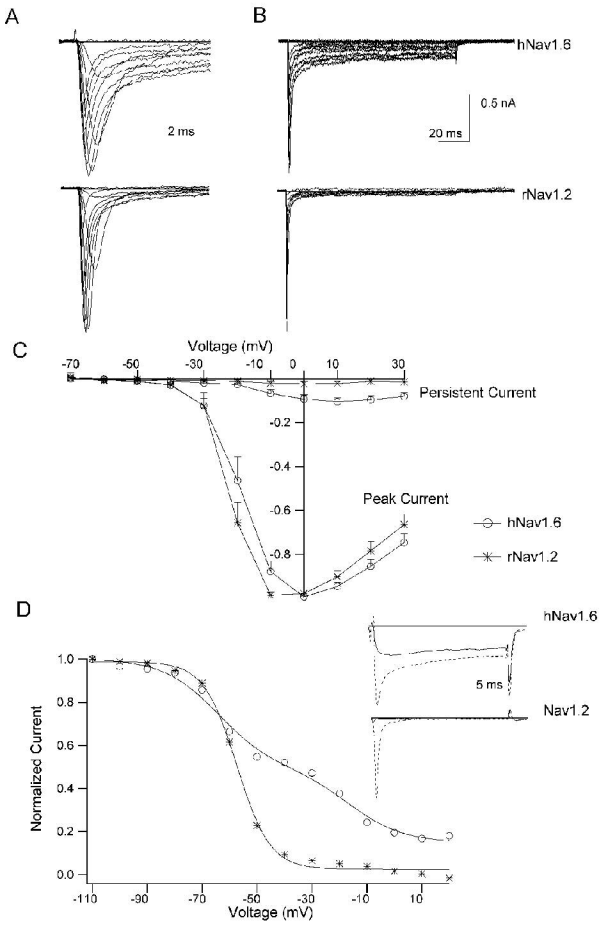

Shirahata et al.

Whole cell Nav currents recorded from tsA201 cells transfected either with hNav1.6 or the rNav1.2 _-subunit. (A, B) Representative traces were elicited by membrane depolarizations for 100 ms ranging from -30 to +50 mV in 10 mV increments from a holding potential of -80 mV. The same trace in (A) is expanded in (B) at a different time scale. The peak sodium curents of hNav1.6 and rNav1.2 were 51.2±1.1 pA/pF (n=30) and 90.0±8.9 pA/pF (n=4), respectively. (C) The current-voltage relationship (I-V curves) of hNav1.6 (_) and rNav1.2 (*). Values were normalized by the maximum amplitude. (D) The voltage dependence of steady-state inactivation and representative traces (insets) for hNav1.6 and rNav1.2. Representative traces with a preconditioning pulse to -110 mV (dotted lines) and -20 mV(solid lines) indicate that the rNav1.2 channel was completely inactivated by a conditioning pulse to -20 mV.

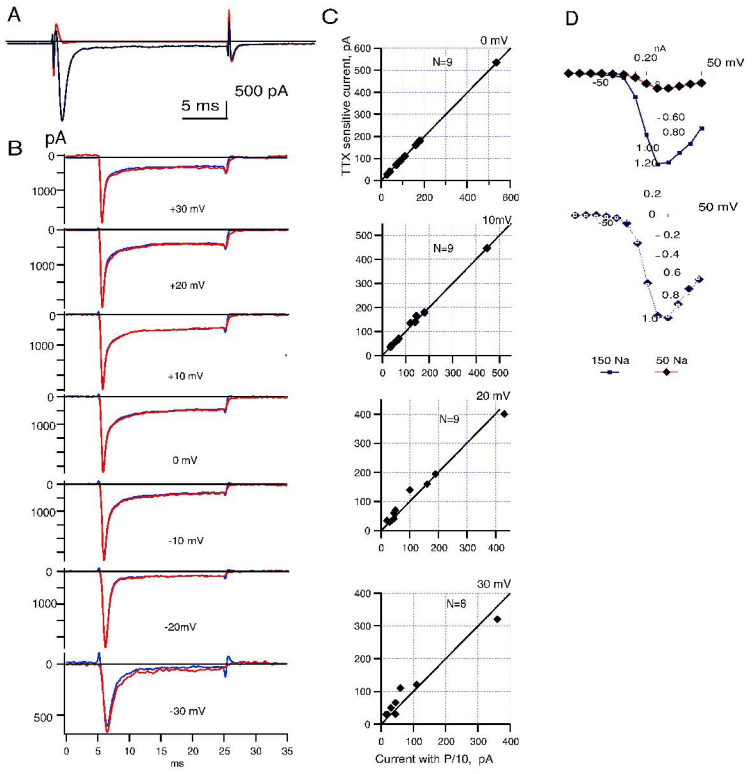

Comparison of inward currents of hNav1.6 between a TTX-sensitive inward current versus a current measured with P/N protocol. A. An example of raw traces before (black) and after (red) application of TTX. Capacitative current and leakage are not corrected. B. Representative traces from one cell at different membrane potentials. Blue indicates the trace obtained with TTX-subtraction and red indicates that with the P/10 protocol. C. X-Y plot of current amplitudes of Ina-p obtained with P/10 and TTX-subtraction from eight cells expressing hNav1.6 cDNA. Data of 0 mV, +10 mV, +20 mV were from 9 cells. Data of 30 mV was from 8 cells. D. The I-V curve of transient inward currents compared under 150 mM sodium and 50 mM sodium. In the lower plot, current amplitude was normalized by the peak value.

Figure 3

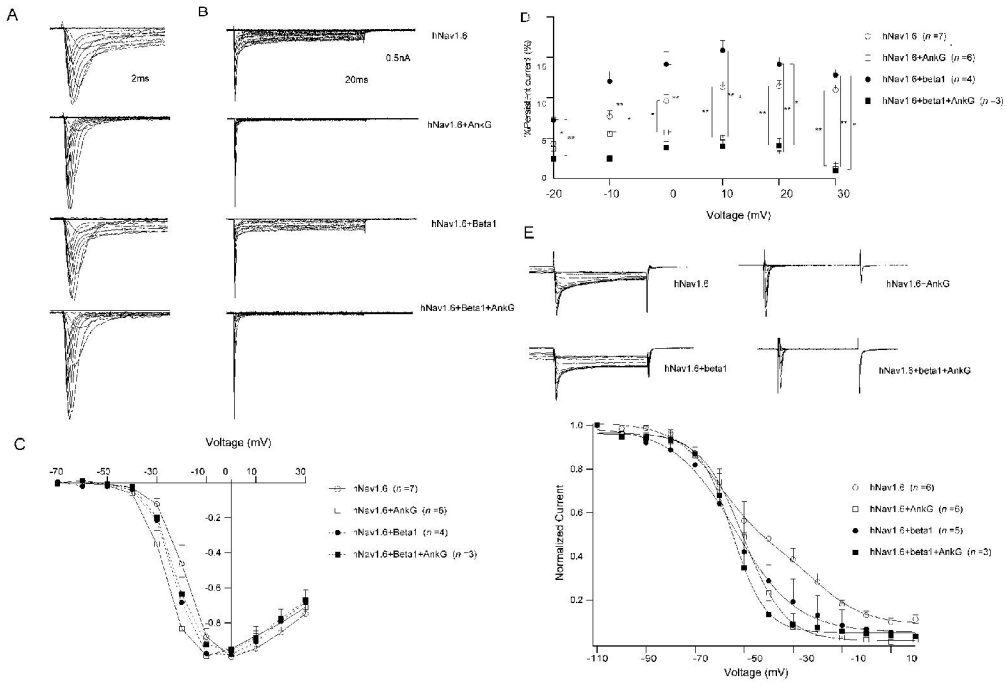

Shirahata et al.

Whole cell sodium currents recorded from tsA201 cells expressing the hNav1.6 _-subunit alone or with ankyrin-G (AnkG) or/and _1-subunit. (A, B) Maximum amplitudes of sodium currents from cells expressing hNav1.6 alone, hNav1.6+AnkG, hNav1.6+_1, and hNav1.6+AnkG+_1 were 51.2±1.1 pA/pF (n=30), 45.3±0.85 pA/pF (n=28), 87.9±12.2 pA/pF (n=6), 78.3±14.9 pA/pF (n=4), respectively. The same records in (A) are shown in a different time scale in (B). (C) The I-V curves obtained from cells transfected with Nav1.6 alone (_), hNav1.6+AnkG(_), hNav1.6+_1 (_), or hNav1.6+_1+AnkG (_). (D) Voltage dependence of the proportion of Ina-p (%pc). Without AnkG, %pc was larger (*; p<0.05, **; p<0.01). (E) The steady-state inactivation curve. Current traces during the test stimuli are shown (the upper panel). The curve of cells expressing AnkG was fitted with a single Boltzmann equation.

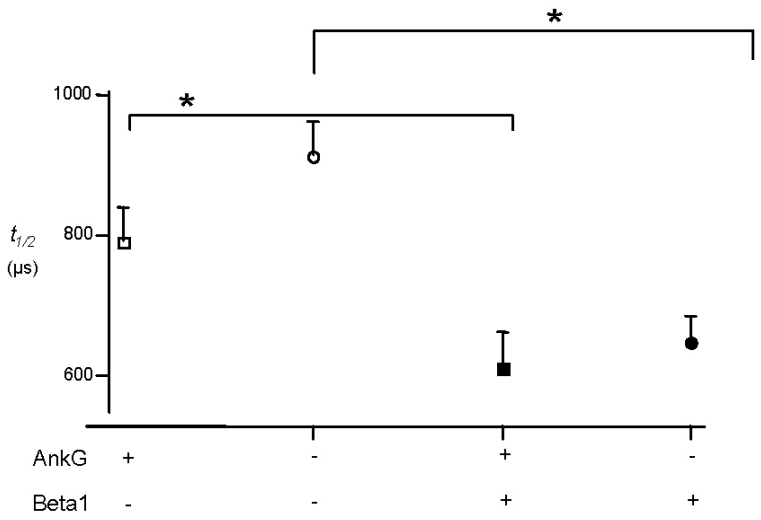

Rising time to half the peak amplitude (t1/2) was determined for cells expressing hNav1.6 alone and cells coexpressing Nav1.6 with ankyrin-G and/or the sodium channel □$B&B□(B1-subunit. The t1/2 of hNav1.6 alone (□$B!{□(B), hNav1.6 plus ankyrin-G (□$B""□(B), hNav1.6 plus □$B&B□(B1 (□$B!|□(B), and hNav1.6 plus ankyrin-G plus □$B&B□(B1 (□$B"#□(B) were 912□$B!^□(B54 ?s (n=13), 789□$B!^□(B50 ?s (n=13), 647□$B!^□(B37 ?s (n=5), and 611□$B!^□(B52 ?s (n=4), respectively. Asterisks indicate significant difference.

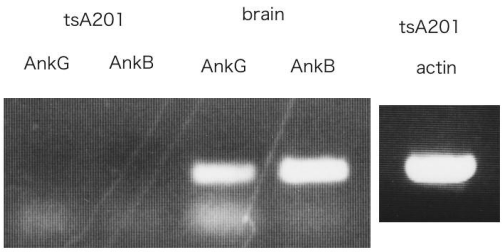

Fig.5 Shirahata et al.

RT-PCR shows no endogenous expression of ankyrin-G or -B gene in tsA201 cells. Right two lanes denote no signal from tsA201 cDNA, but the third and fourth lane shows clear positive signals from brain cDNA. Integritiy of cDNA was checked by the expression of actin (right lane).

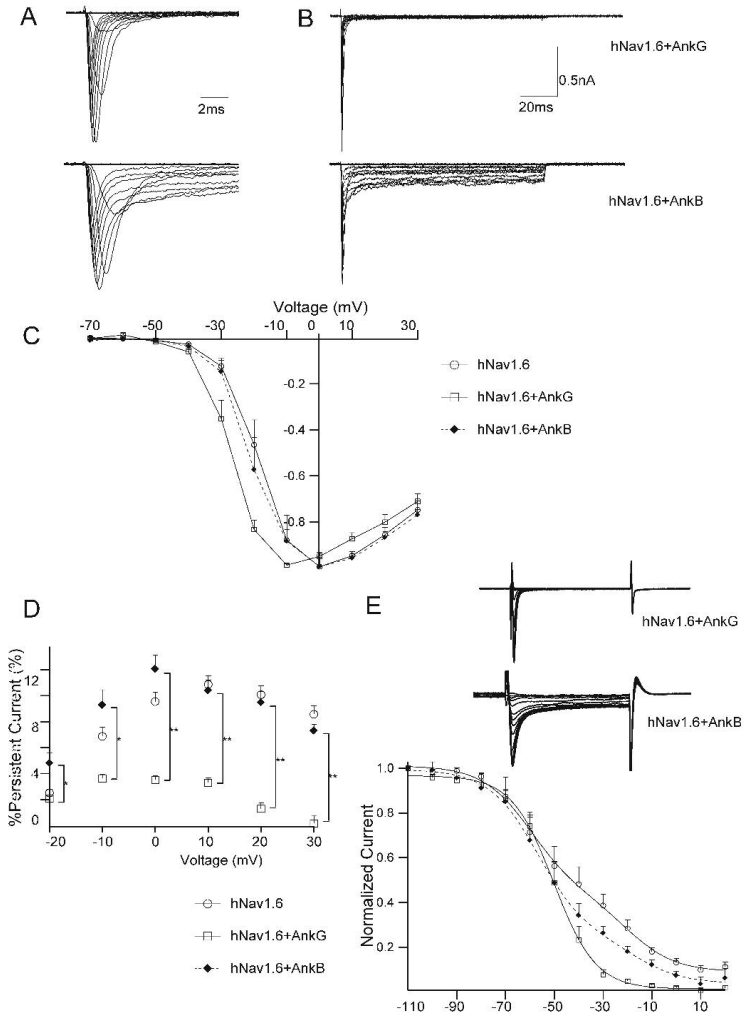

Shirahata et al. Fig.6

Distinct effect between ankyrin-G (AnkG) and ankyrin-B (AnkB) on the Ina-p of the hNav1.6 channel. (A,B) Representative traces are shown with distinct time scale. Maximum current densities of Nav channel currents from cells expressing hNav1.6 alone, hNav1.6+AnkG, and hNav1.6+AnkB were 51.2±1.1 pA/pF (n=30), 45.3±0.85 pA/pF (n=28) 51.3±5.7 pA/pF (n=9), respectively. (C) The I-V curves from cells expressing hNav1.6 alone, hNav1.6 and AnkB (_) and hNav1.6 and AnkG (_). (D) %pc at different membrane potentials (*; p<0.05, **; p<0.01) (E) The steady-state inactivation curve. Current traces during the test stimuli are shown (the upper panel). Fitting the curve from cells coexpressing with AnkB (_)(n = 5) required two components of the Boltzmann equation.

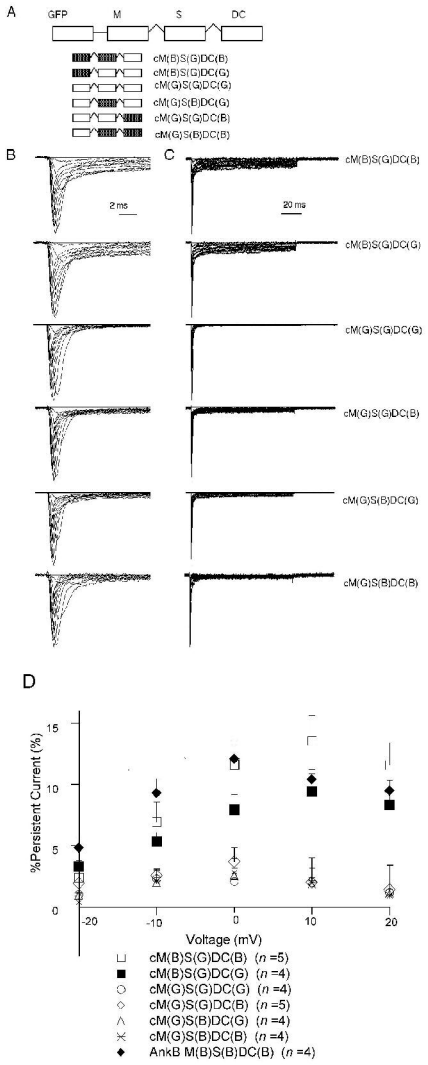

Shirahata et al.

Effect of coexpression of ankyrin-B/G chimeras on the Ina-p of Nav1.6. (A) The scheme of ankyrin-B/G chimeras. (B, C) Representative traces recorded from tsA201 cells expressing ankyrin-B/G chimeras. Maximum current densities of Nav channel currents were not significantly different among chimeras. (D) %pc at distinct membrane potentials.

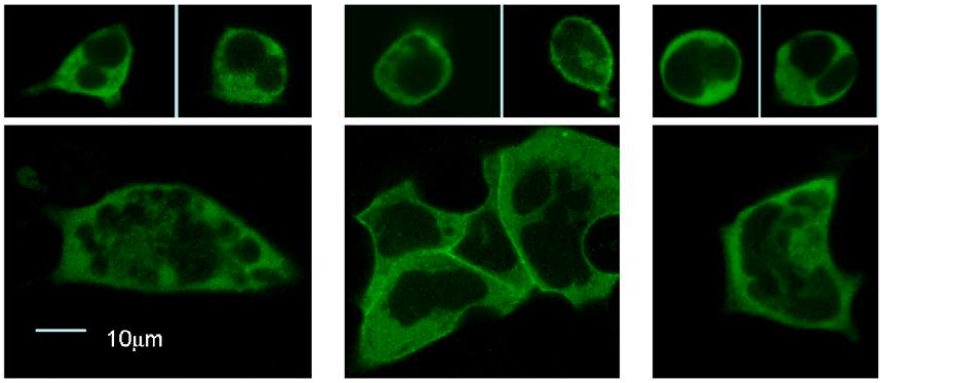

Shirahata et al. Fig. 8

Localization of ankyrin protein analyzed by confocal microscopy. Cells were transfected with hNav1.6 and GFP-fused ankyrin-G. Note that signal is most abundant at the pheriphery of cells (middle panel), whereas signal was more diffuse when ankyrin-G alone or ankyrin-B was expressed.

Table 1. Comparison of proportion of Nav1.6-derived Ina-P from cells transfected with ankyrin-G-B chimeras against cells transfected with ankyrin-B (BBB)

	BBB♦	BGB□	BGG■	GGG○	GGB◊	GBGΔ	GBB*
+20 mV	7.3±0.5%	8.8±1.5%	6.5±1.0%	0.1±0.3%(**)	0.3±0.7%(**)	0.3±0.4%(**)	0.1±0.7%(**)
+10 mV	9.5±0.9	11.6±1.8	8.3±1.3	1.2±0.2(**)	1.4±0.5(**)	1.0±0.4(**)	0.9±0.9(**)
0 mV	10.4±0.8	13.5±2.1	9.4±1.4	2.0±0.2(**)	2.0±0.5(**)	1.8±0.6(**)	1.9±1.2(*)
-10 mV	12.1±1.1	11.6±2.1	7.9±1.3	2.1±0.2(*)	3.7±0.3(*)	2.6±0.6(**)	2.8±1.2(*)
-20 mV	9.3±1.2	6.9±1.6	5.3±0.7	2.3±0.2(**)	2.5±0.1	1.9±0.4(*)	2.1±-0.8
N	4	5	4	4	5	4	4

** P<0.01, * P< 0.05